

To be published in Journal of the Optical Society of America A:

Title: Vortex Analysis in Dynamic Speckle Images

Authors: Gonzalo Sendra, Héctor Rabal, Ricardo Arizaga, and Marcelo Trivi

Accepted: 7 October 2009

Posted: 8 October 2009

Doc. ID: 116650



Vortex Analysis in Dynamic Speckle Images

Gonzalo H. Sendra,^{1,2,*} Héctor J. Rabal,¹ Ricardo Arizaga,¹ and Marcelo Trivi¹

¹*Centro de Investigaciones Ópticas (CONICET La Plata – CIC) & UID Optimo, Area de Ciencias Básicas, Facultad de Ingeniería, UNLP. PO Box 3, 1897 Gonnet, La Plata, Argentina.*

²*Laboratorio Laser, Facultad de Ingeniería, Universidad Nacional de Mar del Plata. Juan B. Justo 4302, 7600 Mar del Plata, Argentina.*

**Corresponding author: ghsendra@ciop.unlp.edu.ar*

Optical vortex analysis has become an important tool in optical metrology. It has been shown to be able to measure small displacements with up to nanometric precision. In this paper we analyze optical vortex behavior in dynamic speckle patterns with boiling phenomenon. We first study translational patterns with boiling and we find the limitations of the optical vortex metrology. Pure boiling patterns were also evaluated and we found a quantitative descriptor for the activity. We also observed that vortices exhibit a Brownian motion in pure boiling patterns. Numerical and experimental results are shown.

OCIS codes: 120.6150, 030.6140, 100.5070, 100.2000.

1. INTRODUCTION

Phase singularities are important features common to all waves. Waves that possess a phase singularity and a rotational flow around the singular point are called vortices. Vortices play an important role in many branches of physics, even those not directly related to wave propagation. Nye and Berry [1], in 1974, described the basic properties of dislocations in wave trains in what

is now known as ‘singular optics’. In a light wave, a phase singularity forms an optical vortex where the wave rotates around the vortex core in a given direction. At its centre, the velocity of this rotation is infinite and the light intensity vanishes. Such points are also referred to as wave-front screw dislocations; because the phase gradient direction swirls around the singular line much like fluid in a whirlpool.

The study of optical vortices and associated localized objects is extremely important from the viewpoint of both fundamental and applied physics. The unique, robust nature of vortex fields is expected to lead to applications in areas that include optical data storage, distribution, and processing. They have recently been shown to provide excellent tools for measurements of quasi static deterministic displacements with, in some cases, obtaining nanometric precision [2, 3].

Dynamic speckle is a stochastic phenomenon, where one of its possible origins is the movement of scatters within or on the surface of a sample when illuminated with laser light. During a slow movement of the sample, upon suitable optical conditions, the structure of the pattern is preserved and can be recognized in successive images, but in samples presenting surface activity, the intensity pattern changes as the sample properties change. This dynamic speckle phenomenon is present in many applications such as biological tissues and industrial processes [4]. Tracking the speckle features provides a means to monitor the time evolution of phenomena and systems under observation; examples include corrosion phenomena, efflorescence, drying of polymers and coatings, and live biological samples. The timescale of the dynamic behavior depends on the physical phenomena that produce the activity.

Vortices are present in any speckle pattern, but they are discarded when the CCD cameras only register space averaged intensity patterns. Recently, Wang et al [2, 3] proposed a

complex representation of the real-valued speckle pattern intensity by means of complex filters. Although the complex representations of real-valued speckle patterns do not introduce any new information, such transforms effectively exploit the existing one. The newly introduced pseudoamplitude and pseudophase associated with the complex signal provide more effective means for analyzing, processing and understanding the available information from the recorded speckle pattern.

This technique was applied to the measurement of nanometric displacements with high resolution [2, 3]. The core structure of each singularity was characterized in terms of its eccentricity, angle between real and imaginary zero crossing lines, vorticity and topological charge. These features were used as “fingerprints” to identify a displaced vortex, even in the case of a large object displacement [2]. Wang et al [5] developed a novel approach to characterize vortices by the analysis of the analogy between the gradient field of the complex signal and the polarization field of a vector wave. They used the Poincaré sphere representation to characterize the phase singularities and found that singularities can be uniquely identified even in a complicated environment.

Optical metrology of vortices from coherent speckle patterns has been mainly oriented to displacement measurements. When we analyze dynamic speckle patterns generated by active samples the speckle grains usually do not experiment translation but deformation, known as ‘boiling’ [6]. There are several methods and techniques to analyze speckle activity in such cases [4], but they are not always suitable for slow dynamic patterns. Besides, many of the techniques require the use of several images, limiting the measurements to only stationary phenomena.

In this work we studied vortices in dynamic boiling speckle patterns. We analyzed the cases of translational with boiling and pure boiling patterns, both obtained from the slow

translation of a rigid diffuser [6], trying to find a correlation between the vortex behavior and the diffuser velocity. We considered several diffuser velocities, but for each of them only two consecutive frames were used to find a descriptor for the diffuser velocity.

2. THEORY

A. Dynamic speckle reference patterns

We used controlled dynamic speckle patterns to evaluate the vortices behavior [6]. These patterns were experimentally and numerically obtained (see next sections) from the displacement of a diffuser in conditions of translational with boiling and pure boiling speckles [7]. The employed geometry is described in Fig. 1 where the lens was only considered for pure boiling patterns. The condition for pure boiling [7] is:

$$\left(\frac{1}{d_o} + \frac{1}{d_i} - \frac{1}{f} \right) \left(1 + \frac{d_o}{\rho} \right) - \frac{1}{d_o} = 0 \quad (1)$$

where ρ is the curvature radius of the illumination wave front. In our case we chose $d_o = d_i = f = 50$ cm and $\rho = \infty$ (plane wave front). We used also object and lens pupils with a diameter of 6 mm and 1 cm respectively.

For the case of translational speckle with boiling we did not consider the lens and we used $z = 50$ cm (object to detection plane) and an object pupil diameter of 5 mm.

B. Complex representation of a speckle pattern

Optical vortices are phase singularities that are exhibited by the optical field. Although CCD cameras only register the intensity of the field, it is possible to obtain a complex signal representation of the intensity by means of complex filters [2, 3]. In our case we used Laguerre-

Gauss filter [2] and all the registered and simulated images were associated to a complex-valued signal by:

$$\tilde{g}(x, y) = \iint_{\infty} H_{LG}(\xi, \eta) G(\xi, \eta) \exp[j2\pi(x\xi + y\eta)] d\xi d\eta \quad (2)$$

where $G(\xi, \eta)$ is the Fourier transform of the intensity speckle pattern $g(x, y)$, and $H_{LG}(\xi, \eta)$ is a Laguerre-Gauss (L-G) filter in the frequency domain defined as follows:

$$H_{LG}(\xi, \eta) = (\xi + j\eta) \exp\left(-\frac{\xi^2 + \eta^2}{\omega^2}\right) \quad (3)$$

The L-G filter acted as a band-pass filter that avoided the appearance of unstable phase singularities due to noise. The density of pseudophase singularities was controlled by choosing the proper bandwidth of the L-G filter function with the ω parameter to approximate the desired mean speckle grain diameter.

C. Analysis and characterization of the core structure of vortices

The pseudophase singularities (vortices) are points where the real and imaginary parts of $\tilde{g}(x, y)$ are zero. However, due to the spatial sampling, the singularities were masked and they had to be located as simultaneous zero crossing points of both real and imaginary parts of the complex signal. Therefore, the first step in the singularities detection is the calculus of the zero crossing lines:

$$\text{Re}[\tilde{g}(x, y)] = 0, \quad \text{Im}[\tilde{g}(x, y)] = 0 \quad (4)$$

After that, the real and imaginary parts of the complex 2-D signal in the vicinity of the pseudophase singularity was suitable approximated by planes [3] as

$$\operatorname{Re}[\tilde{g}(x, y)] = a_r x + b_r y + c_r, \quad \operatorname{Im}[\tilde{g}(x, y)] = a_i x + b_i y + c_i \quad (5)$$

where the coefficients $a_r, b_r, c_r, a_i, b_i, c_i$ were obtained by the least-square fitting method using the pixels surrounding the phase singularity. Its location, with subpixel accuracy, can then be better estimated at

$$x = \frac{c_i b_r - c_r b_i}{a_r b_i - a_i b_r}, \quad y = \frac{a_i c_r - a_r c_i}{a_r b_i - a_i b_r} \quad (6)$$

Each vortex can be characterized by its core structure parameters [2], which are topological charge, vorticity, eccentricity and angle between the real and imaginary zero crossing lines. Besides, there is another way for characterizing the core structure through a Poincaré sphere representation [5] with the following parameters:

$$\begin{aligned} S_0 &= a_r^2 + b_r^2 + a_i^2 + b_i^2, \\ S_1 &= a_r^2 + a_i^2 - b_r^2 - b_i^2, \\ S_2 &= 2(a_r b_r + a_i b_i), \\ S_3 &= 2(a_r b_i - a_i b_r) \end{aligned} \quad (7)$$

which are mathematically analogous to the Stokes parameters in polarization.

Vortex features are used to locate homologous vortices in a pair of frames. In our case we used the Poincaré sphere representation in combination with the topological charge q which is defined [2] as

$$q = \operatorname{sgn}(\vec{\Omega} \cdot \hat{k}) = \operatorname{sgn}(a_r b_i - a_i b_r) \quad (8)$$

where Ω is the vorticity.

The location of a homologous vortex needs of two stages. The first one consists in pre selecting possible homologous vortices by means of one or more thresholds in the variation of some vortex features or in the allowed displacement in the Euclidean or Poincaré space. Subsequently, a merit function is defined and calculated for each surviving vortex. The homologous vortex is then chosen as the one with the least merit function. In our case we used the distance in the geodesic line between two points of the Poincaré sphere as the merit function [5], which is defined as:

$$|\Delta\vec{S}| = \left| \arccos(\vec{S} \cdot \vec{S}') \right| \quad (9)$$

where the primed parameter corresponds to the singularity in the second frame.

The allowed vortex deformation can be increased by using higher thresholds. However, high thresholds increase the possibility of wrongly identified vortices. Hence, thresholds have to be empirically selected considering this compromise relationship. In our case we used a combination of thresholds depending on the analyzed situation: horizontal and vertical displacement (u_h and u_v), Euclidean distance (u_d), Poincaré distance (u_p), and the condition that both homologous vortices share the same topological charge [2]. Finally, we chose the homologous vortex as the one having the minimum Poincaré distance (merit function).

3. EXPERIMENTS

Controlled dynamic speckle patterns were experimentally obtained using the scheme of Fig. 1 where the object plane consisted of a ground glass diffuser [6]. The conditions and geometrical experimental parameters for pure boiling speckle patterns and for translational speckle patterns

with boiling were reproduced from the work of Sendra et al [6]. In the second case we used free propagation geometry and the lens was omitted.

A lensless CCD Pulnix TM 6CN camera connected to a personal computer with a frame grabber was used to record the images that were digitized to 256 intensity levels (8 bits). The displacement of the ground glass diffuser was performed by using an Aerotech ARS 302 MM and a stepping motor (2 μm per step). Different diffuser velocities were obtained by modifying the number of steps between consecutive frames. In our case we used multiples of 10 μm .

4. SIMULATIONS

We carried out simulations using the model of Sendra *et al* [6] to reproduce the experimental patterns. The experimental parameters were the same as the experiment. The image matrix was chosen as 2048×2048 pixels with a spatial sampling of $10 \times 10 \mu\text{m}$ at the detection plane. The diffuser was displaced multiples of 3.33 μm between frames for pure boiling patterns and 10 μm for translational with boiling ones [6].

We also made simulations of completely uncorrelated patterns using the geometry parameters for pure boiling. In this case we employed the same specification described before but with completely uncorrelated random matrices as diffusers.

5. RESULTS AND DISCUSSION

A. Translational Speckle Patterns with Boiling

First, we deal the case of translational with boiling speckle patterns. This case differs from the works of Wang et al [2, 5] in that now there are variations on the parameters of the vortices core structure due to the boiling effect. We tried out the same procedure used by Wang et al. in Ref.

[2], but with the threshold and merit functions based on the Poincaré sphere [5]. Another difference with that work is that we will show results for different displacements obtained by a non supervised algorithm.

The analysis was applied twice. The first time only the Poincare distance threshold was used and the homologous vortex location was estimated by detecting the peak in both the horizontal and vertical displacement histograms. The second time, horizontal and vertical thresholds were included to limit the exploration in a 10x10 pixels square around the estimated location [2]. The Poincare distance threshold was empirically set to $u_p=0.25$ to allow some deformation in the speckle grains. A high correlation was found between the simulated and experimental displacements of the vortices. The number of identified vortices decreases in a similar way for both cases (Fig. 2a). It can be seen in Fig. 2b and 2c that noticeable errors in the measurements are present for some high diffuser displacements. The source of these errors is the miss-identification of vortices due to the finite size of the image that produce a spreading of the displacement histograms and cause inaccuracy in the peak detection. However, in all the miss-estimated displacements, the proportion number of identified vortices was lower than the 8% of the total detected vortices.

So, we can use the number of identified vortices as a control of the measurement. These measurements may be improved if they are not carried out automatically or if there is some prior knowledge about the displacement, i.e. approximated value or direction of the movement.

B. Pure Boiling Speckle Pattern

When we observe a pure boiling speckle pattern, there is no appreciable translation of the speckle pattern as a whole. Speckle grains undergo random deformations and small

displacements. It presents a problem at the moment of identifying homologous vortices because we have no parameter capable of being used as a fingerprint.

Hence, before studying pure boiling patterns we analyzed the behavior of vortices in simulations of completely uncorrelated patterns. This is the worst situation where we would not expect the identification of any homologous vortices. We used the absolute Euclidean displacement u_d as the only threshold and the Poincaré sphere displacement as the merit function. We evaluated four speckle sizes (synthesized complex signal). Table 1 shows the number of detected vortices, the proportion of identified ones, their Euclidean displacement and Poincaré sphere displacement.

Examining this table we can observe that the proportion of identified vortices never takes a zero value. The number of detected vortices increases as speckle size diminished. Although we want a large number of vortices to obtain good statistic, it implies a high density of vortices that augment the probability of miss identifications. The absolute displacement threshold limits uncorrected identifications, but it also establishes a bound in the vortices freedom to move. We should also choose the speckle size and threshold that produce the least proportion of miss identified vortices. Therefore, there is a compromise between the number of detected vortices to obtain a good statistic, the proportion of allowed miss identified vortices and the displacement threshold.

We then decided to use only one threshold in the Euclidean Distance u_d , neglecting any possible vortex creation or destruction. For the analysis of different diffuser velocities we adopted a speckle size of $400 \mu\text{m}$ and an absolute displacement threshold of $u_d = 100 \mu\text{m}$. According to Table 1, it implies that the proportion of identified vortices should be higher than 0.26 to ensure that we are not in the case of miss identified vortices. Nevertheless, we will adopt

twice this amount, i.e. 0.52, to guarantee a better number of correct identifications. On the other hand, we should expect Euclidean and Poincaré sphere displacements smaller than $65.6 \mu\text{m}$ and 0.86 respectively (Table 1).

Simulations and experiments of pure boiling patterns are compared in Fig. 3. The proportion of identified vortices is shown in Fig. 3a. In contrast with the previous case of translation with boiling, it has higher values due to the previous knowledge of slow movement of vortices that ensures a better identification. As these values are higher than 0.52 we can assume that there are a good number of well identified vortices. The average Euclidean distance between homologous vortices is observed in Fig. 3b. It shows a high correlation between experimental and simulated results, but with a non linear response, and it is always smaller than $65.6 \mu\text{m}$. We also confirmed that the mean Poincaré sphere displacement was smaller than 0.86 for all the diffuser displacements.

If we consider that the vortex displacements in pure boiling simulations have random directions, we can treat their movement as a Brownian motion [8]. A feature of the plane Brownian motion (as a random walk) is that the total averaged displacement d_T after N_l time-intervals of displacements of length l is:

$$d_T = l\sqrt{N_l}, \quad (10)$$

We do not know the value of l but we know that it is directly proportional to the minimum averaged Euclidean distance. Hence if we plot the product of the averaged Euclidean distance times the squared root of the diffuser velocity versus the diffuser velocity we should obtain a straight line and this result is evidenced in Fig. 4a. For velocities higher than $75 \mu\text{m}/\text{frame}$ there are numerous miss-identifications of homologous vortices and this method cannot be applied. In

the first range, for velocities lower than $75 \mu\text{m}/\text{frame}$ this measurement is a very accurate descriptor with a linear response as it is zoomed in Fig. 4b. We carried out a linear regression in this region and we found a model $y = 3.5472x$ with $r^2 = 0.9986$. We considered the highest error to establish a confidence bound and estimate the diffuser displacement resolution in $3.14 \mu\text{m}$.

6. CONCLUSIONS

In this work we found that the optical vortex metrology developed by Wang et al [2, 5] is also applicable in presence of boiling phenomenon, but with a higher Poincaré threshold to allow for speckle grain deformations.

Pure boiling speckle patterns are present in many situations and their activity is usually characterized by different descriptors depending on the application. Nevertheless, these descriptors are not usually suitable in low activity patterns. We found that vortices show Brownian motion and their statistical displacement is a good descriptor for low activities. Besides, this descriptor requires only two frames. The major problem of this analysis is the identification of homologous vortices between frames. Future studies should be focused on the reduction of the number of miss identified vortices.

Results suggest that this descriptor may be also useful for analyzing boiling patterns generated by other phenomena, so that it may be generalized as a quantitative descriptor common to several experimental situations. By means of a soft analogy with particles Brownian motion, the slope of the curve in Fig. 4b could be associated to a kind of “speckle temperature” that would be characteristic of the activity of the considered dynamic phenomenon. This concept will be developed elsewhere.

ACKNOWLEDGEMENTS

This work was supported by CONICET, CIC, Universidad Nacional de La Plata and Universidad Nacional de Mar del Plata, Argentina.

REFERENCES

1. J. F. Nye and M. V. Berry, "Dislocations in wave trains," Proc. R. Soc. Lond. A. **336**, 165-190 (1974).
2. W. Wang, T. Yokozeki, R. Ishijima, M. Takeda, and S. G. Hanson, "Optical vortex metrology based on the core structures of phase singularities in Laguerre-Gauss transform of a speckle pattern," Optics Express **14**, 10195-10206 (2006).
3. W. Wang, T. Yokozeki, R. Ishijima, A. Wada, S. G. Hanson, Y. Miyamoto, and M. Takeda, "Optical vortex metrology for nanometric speckle displacement measurement," Optics Express **14**, 120-127 (2006).
4. H. J. Rabal and R. A. Braga, *Dynamic laser speckle and applications*, Optical science and engineering (CRC Press, Boca Raton, 2009), p. 272.
5. W. Wang, M. R. Dennis, R. Ishijima, T. Yokozeki, A. Matsuda, S. G. Hanson, and M. Takeda, "Poincaré sphere representation for the anisotropy of phase singularities and its applications to optical vortex metrology for fluid mechanical analysis," Optics Express **15**, 11008-11019 (2007).
6. G. Sendra, H. Rabal, M. Trivi, and R. Arizaga, "Numerical model for simulation of dynamic speckle reference patterns," Optics Communications **282**, 3693-3700 (2009).
7. T. Okamoto and T. Asakura, "The statistics of dynamic speckles," Progress in Optics **34**, 183-248 (1995).

8. B. D. Hughes, *Random Walks and Random Environments* (Clarendon Press, Oxford, New York, 1995), Vol. 1.

Published by

OSA

FIGURE CAPTIONS

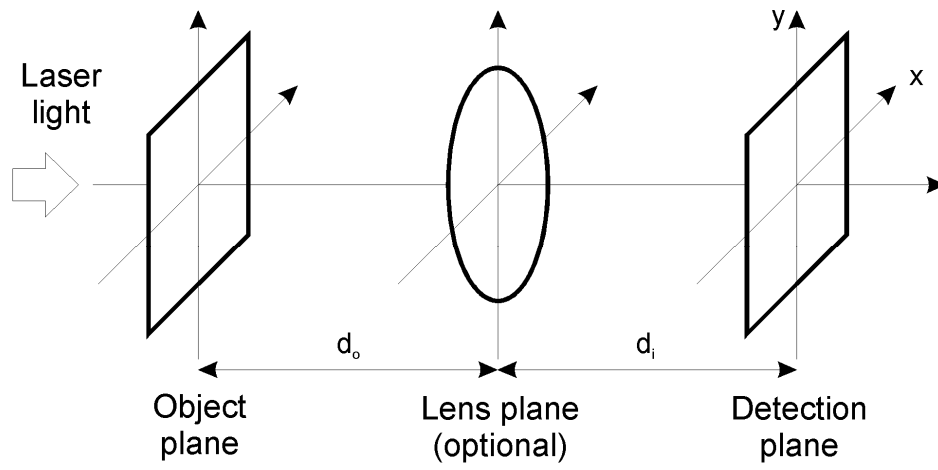
Figure 1. Set-up scheme for simulation and experiment. The object plane is a moving diffuser.

Figure 2. Vortex displacement analysis as a function of the diffuser velocity for simulated and experimental translational speckle patterns with boiling: a) Proportion of identified vortices, b) Mean horizontal displacement, and c) Mean vertical displacement.

Figure 3. Vortex displacement analysis as a function of the diffuser velocity for simulated and experimental pure boiling speckle patterns: a) Proportion of identified vortices, and b) Average euclidean distance between homologous vortices.

Figure 4. Product of the averaged Euclidean distance and the squared root of the diffuser velocity as a function of the diffuser velocity.

Figure 1



PUBLISHED BY

OSA

Figure 2

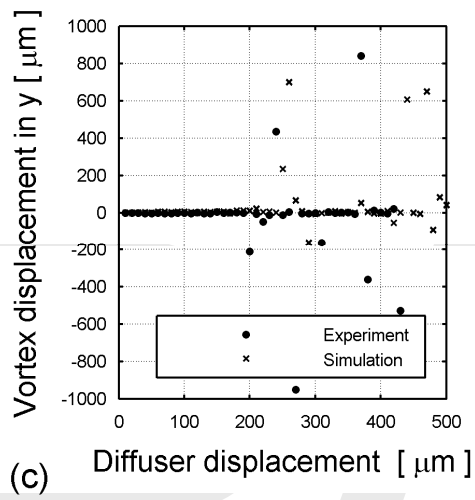
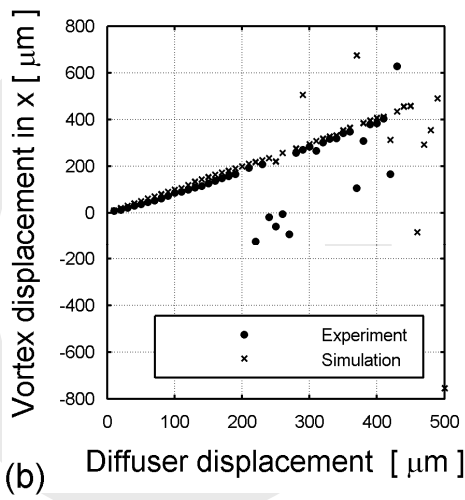
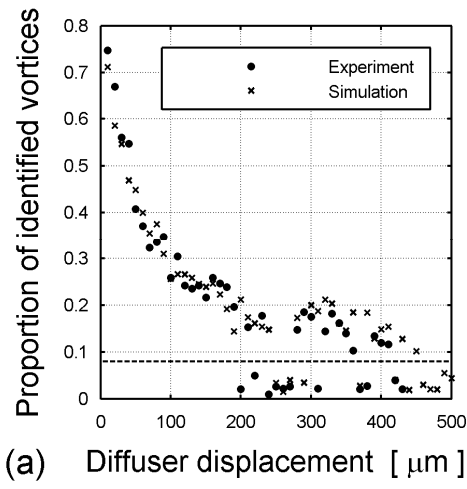
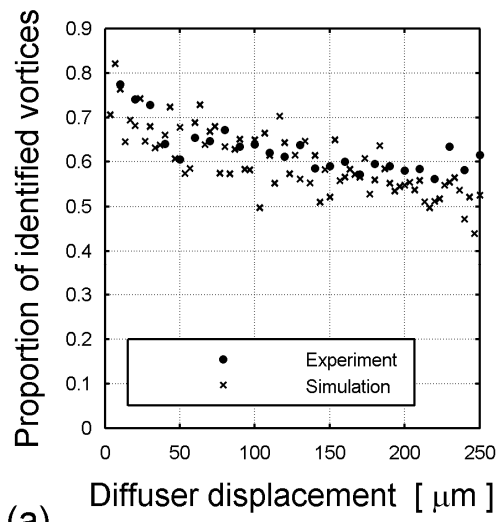
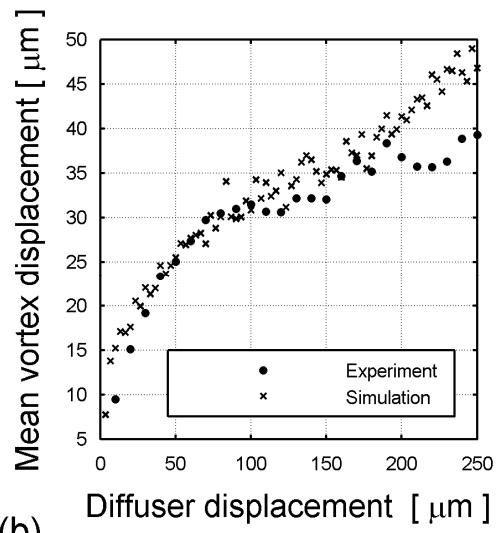


Figure 3



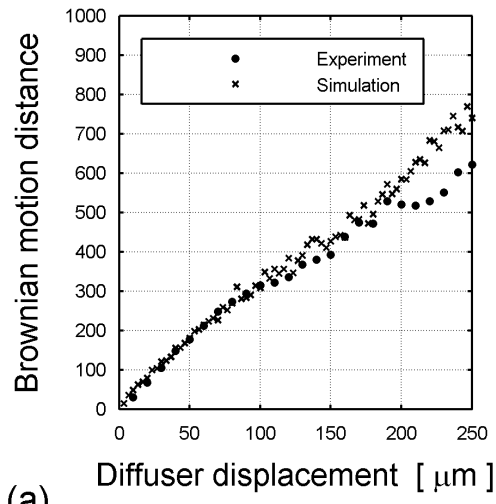
(a)



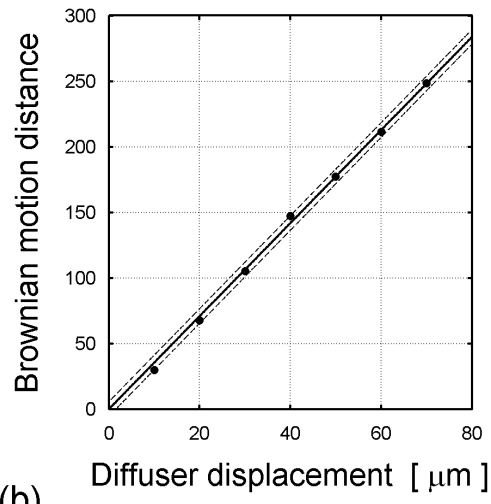
(b)

OSA

Figure 4



(a)



(b)

OSA

Table 1. Vortices behavior in uncorrelated speckle patterns.

| Speckle size ($1/\omega$) | Detected vortices | | Abs. disp. threshold u_d | Proportion of ident. vortices | | Displacement [μm] | | Poincaré sphere displacement | |
|--------------------------------|-------------------|------|-------------------------------|-------------------------------|------|--------------------------------|------|------------------------------|-------|
| | mean | std | | Mean | Std | Mean | Std | mean | Std |
| 200 μm | 817.0 | 31.7 | 50 μm | 0.24 | 0.01 | 33.0 | 0.74 | 0.90 | 0.038 |
| | | | 100 μm | 0.61 | 0.02 | 64.5 | 0.97 | 0.81 | 0.014 |
| | | | 150 μm | 0.74 | 0.03 | 97.0 | 1.20 | 0.71 | 0.013 |
| 300 μm | 373.8 | 19.5 | 50 μm | 0.13 | 0.02 | 33.3 | 1.2 | 0.96 | 0.047 |
| | | | 100 μm | 0.42 | 0.05 | 64.7 | 1.9 | 0.91 | 0.019 |
| | | | 150 μm | 0.63 | 0.05 | 95.7 | 3.0 | 0.82 | 0.030 |
| 400 μm | 206.0 | 14.8 | 50 μm | 0.07 | 0.02 | 34.9 | 4.4 | 0.91 | 0.101 |
| | | | 100 μm | 0.26 | 0.03 | 65.6 | 4.6 | 0.86 | 0.074 |
| | | | 150 μm | 0.49 | 0.04 | 97.6 | 4.8 | 0.84 | 0.038 |
| 500 μm | 130.3 | 7.9 | 50 μm | 0.05 | 0.02 | 33.6 | 2.9 | 0.88 | 0.098 |
| | | | 100 μm | 0.19 | 0.04 | 66.0 | 5.8 | 0.94 | 0.045 |
| | | | 150 μm | 0.36 | 0.04 | 96.7 | 5.8 | 0.92 | 0.068 |